INL/EXT-18-51694
Revision 0

Transition of Spent Nuclear Fuel to Dry Storage

Milestone 1
Task 1.2 Report

Modeling activities concerning aluminum spent nuclear fuel cladding integrity

Michael V. Glazoff
Tedd E. Lister

December 2018

The INL is a U.S. Department of Energy National Laboratory
operated by Battelle Energy Alliance

DISCLAIMER

This information was prepared as an account of work sponsored by an agency of the U.S. Government. Neither the U.S. Government nor any agency thereof, nor any of their employees, makes any warranty, expressed or implied, or assumes any legal liability or responsibility for the accuracy, completeness, or usefulness, of any information, apparatus, product, or process disclosed, or represents that its use would not infringe privately owned rights. References herein to any specific commercial product, process, or service by trade name, trademark, manufacturer, or otherwise, does not necessarily constitute or imply its endorsement, recommendation, or favoring by the U.S. Government or any agency thereof. The views and opinions of authors expressed herein do not necessarily state or reflect those of the U.S. Government or any agency thereof.

INL/EXT-18-51694
Revision 0

Transition of Spent Nuclear Fuel to Dry Storage

Milestone 1
Task 1.2 Report

Modeling activities concerning aluminum spent nuclear fuel cladding integrity

Michael V. Glazoff
Tedd E. Lister

December 2018

Idaho National Laboratory
Idaho Falls, Idaho 83415

http://www.inl.gov

Prepared for the
U.S. Department of Energy
Office of Environmental Management
Under DOE Idaho Operations Office
Contract DE-AC07-05ID14517

ABSTRACT

In 2017, a report was prepared by the Spent Nuclear Fuel Working Group in 2017 and titled “Technical Considerations and Challenges for Extended (>50 Years) Dry Storage” [1,2]. In this report several key scientific issues were identified pertaining to the problem of aluminum spent nuclear fuel (ASNF) and its safe removal from wet storage with subsequent drying and transfer to dry storage at the Department of Energy (DOE) Idaho National Laboratory (INL). This report outlines two modeling analyses performed for aluminum and aluminum oxides.

The first analysis examined the solubility of aluminum oxides as a function of temperature and pH. This report presents existing literature produced as far back as the 1950’s and including significant analysis and reporting performed at Alcoa in the 1980’s. The primary technical gap was the lack of solubility data beyond that reported at standard temperature (25°C). The analysis examined these solubility curves as a function of temperature as well as phase type. The pH value of minimum solubility shifted with temperature but was insensitive to the oxide phase type. The solubility increases with temperature as would be expected, where an order of magnitude increase was observed from 25°C and 90°C. This data provides greater information to understand the various conditions experiences by ASNF including in dry storage in cases where water filming may occur.

A second thermodynamic analysis was performed to examine the aluminum phase behavior as a function of temperature. This was performed to understand limitations and possible problems with fuel drying at elevated temperatures. Based on what has been established in previous reports, water remains chemically entrained within boehmite until temperatures exceeding 400°C. Analysis showed that significant phase changes occurred with highly alloyed AA6061 and AA5052 while the more pure aluminum (AA1100) showed nearly ideal behavior (i.e., limited phase changes). In the case of the more alloyed AA5052 and AA6061, the phase changes could take place at relatively low temperatures (100°C to 250°C), and thus may have already experienced some of these phase changes in service. As results are thermodynamic in nature, assessment of kinetics will be examined to determine if the phase changes are a concern for the relatively short fuel drying step.

CONTENTS

FIGURES

TABLES

Transition of Spent Nuclear Fuel to Dry Storage

Milestone 1
Task 1.2 Report

Understanding degradation Mechanisms of aluminum clad fuels: Assessment of Boehmite and Gibbsite Solubility in water

Two possible approaches to solving the problem of assuring the safe interim dry storage of the SNF are discussed. This review considers the SNF condition when it is moved to wet or dry storage and the effect on the SNF from storage conditions. One approach could be tentatively called "Deep Data Mining;" the other one would be based on the application of our knowledge of materials, corrosion science, reactor neutronics and thermo-hydraulics to deal with corrosion issues and possible physical damage arising at different stages of the SNF handling and storage. This approach tentatively could be called "Traditional Science-Based Engineering." It is anticipated that this approach will provide potential users with a predictive tool for the SNF damage assessment. Their relative descriptions are provided below.

1. INTRODUCTION

This report comprises a follow-up technical work done using recommendations and guidance given in [1,2]. It documents our understanding of some of the key factors affecting long-term structural stability of wrought aluminum alloys AA1100; AA5032; and AA6061. These materials, with proper surface treatment forming a thin film of protective boehmite, are used as cladding materials for the U-Al nuclear fuel. The analysis includes the following stages that needed to be considered:

1. In-Reactor Service / Post Discharge Condition
2. Water Cooling
3. Fuel Drying
4. Dry Storage

There is a number of nuclear reactors in the United States and worldwide that use fuel with different aluminum alloy cladding including the Advanced Test Reactor (ATR) at INL. During its life cycle, any given fuel element goes through several working cycles inside the reactor (see above), then it is transferred to the "canal", then to wet storage. Finally, the whole lifecycle culminates in transferring the aluminum spent nuclear fuel (ASNF) from wet storage to dry storage. During all of the operations, ASNF elements are subjected to different types of corrosion, including pitting, crevice, erosion-corrosion, etc. Understanding how the different processing operations affect corrosion rates and products formed on the surface of the fuel elements is very important if the ASNF placement into dry storage is to be conducted properly.

In this section of the report, a research effort is documented aimed at understanding the growth of corrosion products such as duplex films and bayerite, on the surface of a fuel element, which is often protected from corrosion by a 2–3 μm layer of boehmite. In so doing, the classical results by Pourbaix obtained in 1955 were subject to the critical review and analysis. The re-assessment of the boehmite and gibbsite solubility was done for the four sets of conditions corresponding to (1) pure water, as in the original research by Pourbaix; (2) primary cooling circuit at the ATR; (3) storing ASNF elements in the canal; and (4) special conditions. It was established, using the most up-to-date experimental results and electrolyte solution modeling tools that the solubility minima for boehmite, gibbsite, and bayerite occur at different values of pH, not the single value of pH = 5.2 as established at 25°C by Pourbaix in 1955.

Temperature dependence of solubility was studied as well and demonstrated a significant shift in the values of pH corresponding to the minimum solubility.

1.1 Formulation of the Problem

It is important to answer one fundamental question: what is the concern with aluminum oxide, oxy-hydroxide, and hydroxide dissolution? The reason is that these processes exert a profound influence upon corrosion of aluminum-clad nuclear fuel materials. This effect is well documented and understandable [3,4]. Indeed, with the dissolution of oxides thermal conductivity of the coolant changes as well as that of the fuel elements (locally). In turn, these processes affect the local chemistry and the condition of the protective boehmite film on the surface of fuel elements [3,4]. Therefore, to understand corrosion of Al-clad fuel elements one needs to understand the fundamentals of modern chemistry of aqueous solutions of electrolytes, types of corrosion and how they develop, fundamentals of the metallurgy of aluminum alloys, neutronics, thermo-hydraulics, and more. All this makes the problem of corrosion in nuclear systems interdisciplinary and extremely challenging.

The first systematic study of this important issue (i.e., solubility of aluminum oxides, oxy-hydroxides, and hydroxides) belongs to Pourbaix and his coworkers [5]. It was published in 1955 and, with minor variations, reproduced in the literature until the present time [6]. Pourbaix reviewed the available experimental results and provide a rigorous scientific basis in terms of the chemical speciation of solutions and structure of different aluminum bearing oxides [5]. These included (α–Al_2O_3), oxy-hydroxides (γ-AlO(OH), and hydroxides (α–$Al(OH)_3$ and γ–$Al(OH)_3$). Later, efforts to review and update this information were made by Lawson [7] and other researchers [8-12].

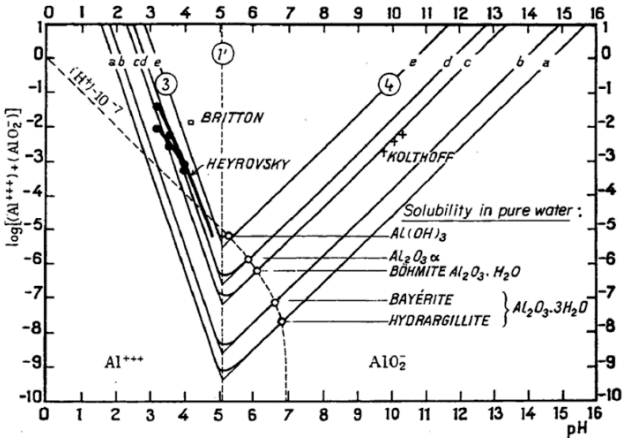

Figure 1. The solubility of boehmite, gibbsite, bayerite, hydrargillite[a] and tabular alumina at 25°C in pure water as a function of pH [5].

One research effort of significant note is the "Alcoa Technical Paper #19" which describes the oxide chemistry of aluminum [8]. It provided an overview of not only the compounds mentioned above, but also a whole class of the so-called "transition aluminas", many of which find application as catalytic supports or catalysts. This report described the complex cascades of structural transformations among different aluminum hydroxides, oxy-hydroxides, and oxides [8]. In particular, he provided the ranges of their thermal stability and emphasized that four such cascades of transformations need to be identified, see Figure 2 [8].

[a] In modern literature, the term "hydrargillite" corresponds to "gibbsite", not to an oxy-hydroxide of aluminum.

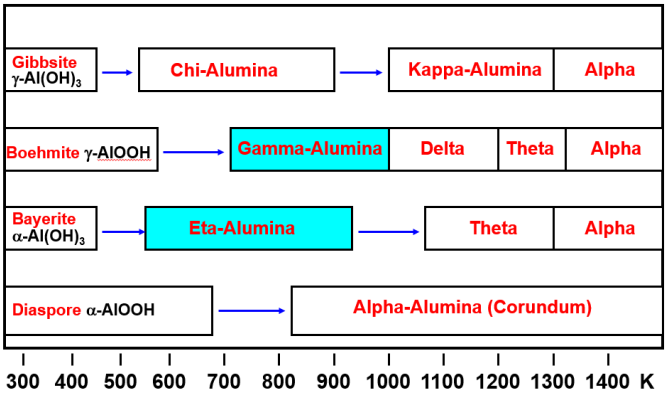

Figure 2. Transformation sequences of aluminum oxides, oxy-hydroxides, and hydroxides [8].

These results have profound implications for the whole lifecycle of ASNF. Indeed, it clearly shows a complete dehydration of the fuel is impossible as the boehmite will transform into γ-Al_2O_3 only at temperatures exceeding 475° – 500°C. However, at such temperature, phase microstructure will change rapidly (see the 2nd part of this report) recrystallization of the AA6061 in the T6 temper would commence. This makes it impossible to complete the dehydration process without profound changes in the alloy microstructure. Additionally, incipient melting of the fuel element cladding may ensue. The same is true with respect to the AA6061 alloy in the O-temper (completely recrystallized [6,13]), which could undergo incipient melting if heated above ~570°C [14]. These important issues need to be verified, which will be done in a separate research effort.

Since the publication of the Alcoa report in 1987, many additional research efforts were made [see, e.g., 9-12]. The second comprehensive overview of the information available about transition aluminas and hydroxides was performed in 2010 by Karamalidis and Dzombak [12]. This work dealt with the issues of the surface complexation of gibbsite and well as other important oxides. The energies of adsorption of different chemical elements upon gibbsite surfaces were determined. This monograph is important because it emphasizes the role of minor additions of the different chemical elements adsorbed from aqueous solutions for subsequent growth of gibbsite. On the surface of a used fuel element, the formation of gibbsite takes place as a result of corrosion phenomena, so it is critical to study this issue in detail.

hcp

$$\alpha\text{-AlOOH (diaspore)} \xrightarrow{700°–800°C} \alpha\text{-}Al_2O_3$$

$$\gamma\text{-Al(OH)}_3\text{(gibbsite)} \xrightarrow{150°–300°C} \chi \xrightarrow{650°–750°C} \kappa \xrightarrow{1000°C} \alpha\text{-}Al_2O_3$$

$$5Al_2O_3\cdot H_2O \text{ (tohdite)} \xrightarrow{700°–800°C} \kappa' \xrightarrow{750°C} \kappa \xrightarrow{900°C} \alpha\text{-}Al_2O_3$$

$$\text{Vapor (CVD)} \rightarrow \kappa \rightarrow \alpha\text{-}Al_2O_3$$

fcc

$$\gamma\text{AlOOH (boehmite)} \xrightarrow{300°–500°C} \gamma \xrightarrow{700°–800°C} \delta \xrightarrow{900°–1000°C} \theta \xrightarrow{1000°–1100°C} \alpha\text{-}Al_2O_3$$

$$\alpha\text{-Al(OH)}_3\text{ (bayerite)} \xrightarrow{200°–300°C} \eta \xrightarrow{600°–800°C} \theta \xrightarrow{1000°–1100°C} \alpha\text{-}Al_2O_3$$

$$\text{Amorphous (anodic film)} \rightarrow \gamma \rightarrow \delta \rightarrow \theta \rightarrow \alpha\text{-}Al_2O_3$$

$$\text{Melt} \rightarrow \gamma \rightarrow \delta,\theta \rightarrow \alpha\text{-}Al_2O_3$$

Figure 3. Common Processing Routes Resulting in Formation of Different Metastable Al_2O_3 Structures and the Sequences of Phase Transformations toward the Stable α-Al_2O_3 Phase [12].

Summarizing these results, the diagrams in Figures 2 and 3 were modified as shown in Figure 4 [12].

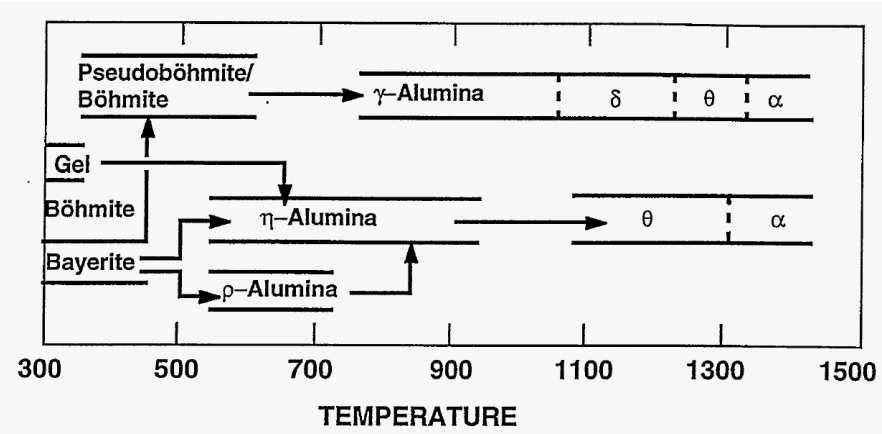

Figure 4. Transformation sequence of the ideal corrosion products expected to be present on the surface of spent ATR fuel elements that have been stored in canals such as ICPP-603 [15,16].

The diagram in Figure 4 attempts to establish the cascades of phase transformations similar to the well-known study by Wefers and Misra [8], Figure 2. However, the origin of these data is not clear and seems to provide just a qualitative picture of transformations.

There are comments in the literature [16] that chemical equilibrium is difficult to achieve in reactions involving the formation of the various hydrated oxides of aluminum. For this reason, the dehydration reaction products are always the most kinetically accessible phases [17]. However, this does not imply that if a certain process is thermodynamically prohibited, it still may proceed on the "kinetical" grounds. What this means is that the rate of the corresponding process, as well as the rates of the competing processes with metastable phases, will vary in a significant range depending on such parameters as the vapor phase composition, heating rate, temperature, and particle size and purity of the original corrosion product.

According to Figure 4, loosely bound water starts to evolve from the surface of water-corroded aluminum at about ~400 K (127°C) [15]. The dehydration of bayerite to form pseudo-boehmite and ultimately boehmite does not start unless the temperature is above 443 K (170°C). Bayerite can be completely dehydrated to ρ-Al_2O_3, a spinel alumina structure, at about 500 K (227°C), while pseudo-boehmite can be transformed to γ-Al_2O_3, another spinel alumina structure, at temperatures around 623 K (350°C). γ-Al_2O_3 is also the crystalline product of thermal oxidation of aluminum metal in the temperature range 723 to 873 K (450 – 600°C), but it contains water in its lattice. Much higher temperatures (>1300 K) are required to form the completely anhydrous corundum structure of alumina.

In this research effort, our goal was to update the 60+ year-old classical results reported by Deltombe and Pourbaix [5], with the goal of ensuring that optimal conditions were selected at all stages of the nuclear fuel operations and storage (chemistry, pH, etc.). Also, it was important to update the chemical speciation of the corresponding aqueous systems (see cases 1-4 above).

1.2 Thermodynamics of Aqueous Solutions

This work was conducted using the software called "Stream Analyzer" by OLI, Inc. [18], employing the most up-to-date thermodynamic databases. The models adopted by OLI allow for the non-ideal nature of aqueous solutions. This is achieved using the Helgeson-Kirkham-Flowers equation of state originally proposed in 1981 [19]. This famous equation was revised and improved in [20]. It was verified extensively for many aqueous electrolyte systems and demonstrates excellent accuracy in terms of calculating partial molar thermodynamic properties of components in such solutions as well as their

solubility. This approach allows for accurately estimating the electrostatic interactions of charged species as well as the short-range order terms (neutral species). The sequence of steps required to perform thermodynamic modeling of a given aqueous electrolyte system, therefore, can be summarized as follows:

1. Write equilibrium mass action for all independent interphase aqueous reactions
2. Write equilibrium equations for the constants of chemical equilibrium
3. Take into consideration to overall neutrality of the system
4. Write mass balance equations to complete the formulation of the problem
5. Solve the resulting set of nonlinear algebraic/differential equations

1.3 Model Validation and Verification

In all situations when any computer modeling system is used to generate scientific results, questions arise about their verification and validity. In this case, validation consists of using different data sets for similar aqueous electrolyte systems and giving the predictions that are close to reliable experimental results.

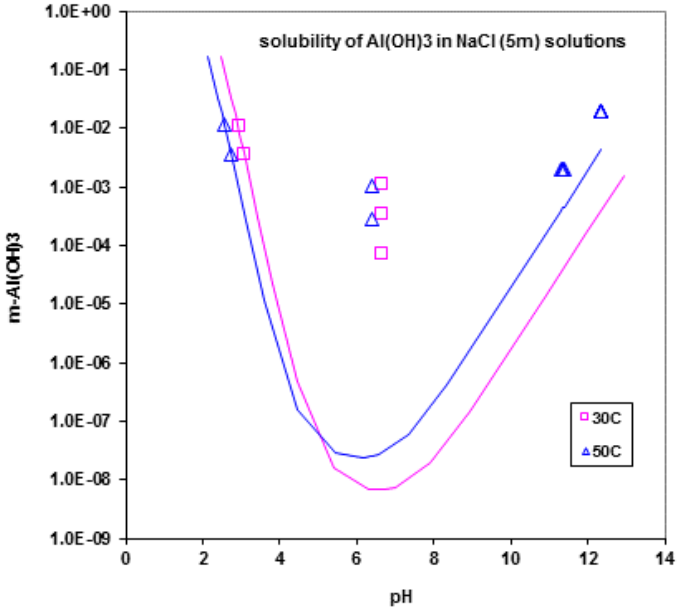

Figure 5. The solubility of gibbsite γ–$Al(OH)_3$ in 5M solution of NaCl in water at different values of pH. Experimental data were taken from [21-22].

One can see from Figure 5 that the agreement with experiment in the areas of acidic pH values (less than 6) and basic values (greater than 10) is very good. However, for neutral values of pH, there is a substantial discrepancy. It is caused by the significant difficulties of experimentation when the solubility of substances is very low [23].

The other system that was considered in this work was $Al(OH)_3$ – NaOH at 25°C. Experimental results were retrieved from publications [21, 24-25]. The hollow blue triangles, squares, and circles correspond to the results from [21, 24-25], correspondingly. The blue solid line represents the results of the OLI Stream Analyzer modeling. All data correspond to the minimal solubility of gibbsite.

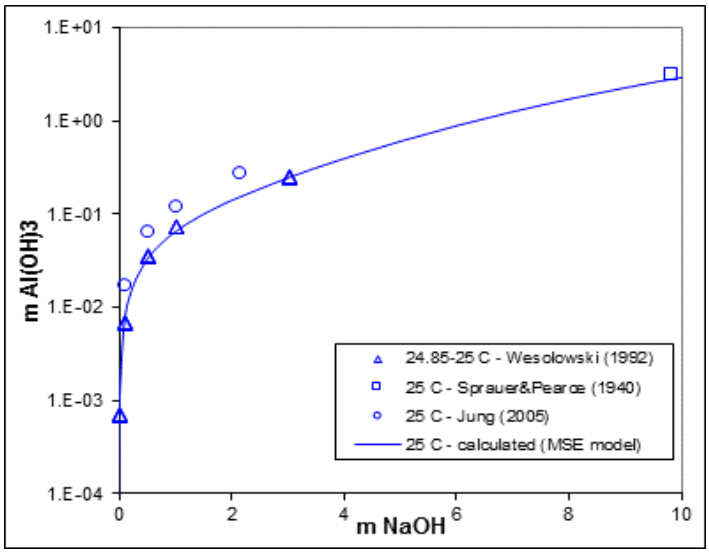

Figure 6. The solubility of gibbsite in aqueous solution of NaOH containg from 0 to 10m of NaOH. The hollow blue triangles, squares, and circles correspond to the results from [21, 24-25], correspondingly. The blue solid line represents the results of the OLI Stream Analyzer modeling. All data correspond to the minimal solubility of gibbsite; temperature 25°C.

The same system was assessed for the case of 50°C [21, 23, 25-26], Figure 7. Some theoretical results supporting our conclusions were found in [27-29].

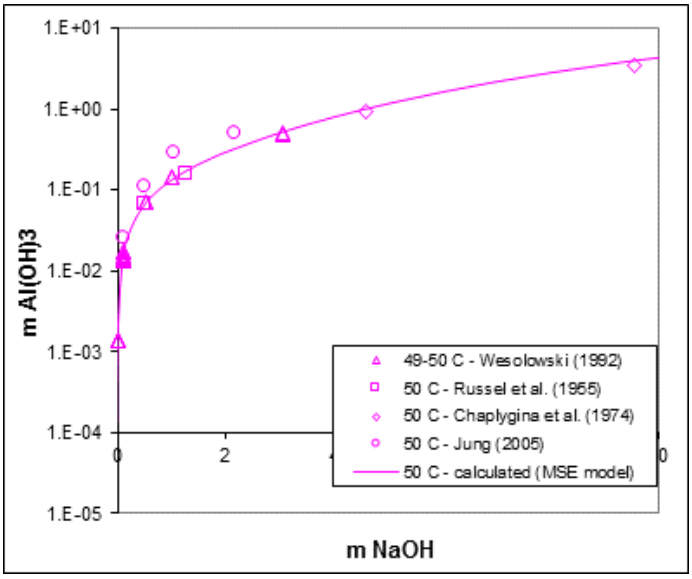

Figure 7. The solubility of gibbsite in the aqueous solution of NaOH containg from 0 to 10m of NaOH. The hollow magenta triangles, squares, rhombs, and circles correspond to the results from [21, 23, 25-26], respectively. The magenta solid line represents the results of the OLI Stream Analyzer modeling. All data correspond to the minimal solubility of gibbsite; temperature 50°C.

On the basis of the conducted validation work, it becomes clear that the Aqueous Electrolyte Model by OLI is quite adequate for a number of systems containing aluminum hydroxide at different values of pH and in a temperature range from at least 25°C to 60°C.

1.4 Modeling of Gibbsite and Boehmite Solubility in Aqueous Environments

In the case of aqueous systems with boehmite and gibbsite, experimental data are available in the literature, in particular, at temperatures 30°C and 50°C [21-22]. Using these experimental results and employing the OLI Optimization Tool, we constructed the first variant of the solubility diagrams, see Figure 8.

One important conclusion is that the chemical speciation of the aqueous environment differs from the description originally given by Deltombe and Pourbaix [5]. The chemical species described in [5] are Al^{3+} in the acidic domain and AlO_2^{-1} in the basic domain of the diagram in Figure 1. Modern chemistry of aqueous electrolyte systems gives a different answer: Al^{+3} (only at very low values of pH) exists as $Al(OH)_2^+$, solid AlO(OH), and $Al(OH)_4^-$.

At any given condition, the OLI Stream Analyzer can only predict a single aluminum oxide (oxy-hydroxide, or hydroxide). For this reason, multiple plots were necessary. Also, the constructed solubility diagrams do not represent true Pourbaix diagrams. Indeed, Pourbaix diagrams are constructed using specified activities of species. A typical choice is that of 10^{-6} M for a particular species concentration in the aqueous phase. In the conducted simulations, it was not possible to hold a specific activity (concentration) because of the specifics of Stream Analyzer software. Instead, the results displayed in Figure 8 were obtained using the so-called "pH survey" with a fixed amount of a highly soluble aluminum salt such as $AlCl_3$ (amounts used from 10^{-6}M to 10^{-3}M).

As it follows from Table 1, In the ATR pressure coolant system (PCS) and lower drywell (LDW) and in the canal, in the normal range the concentration of Cl^- should not exceed 0.05 ppm, while the critical (control) value is equal to 0.1 ppm for the LDW and PCS and is somewhat higher for the canal −0.25 ppm [30]. Therefore, it is necessary to understand how significant this difference is going to be for the modeling results. Looking at the original research published in [5], we see that to get the value of pH to a desirable range, HCl and NaOH were used as titrants. No additions of $AlCl_3$ were made to control the amounts aluminum in the liquid phase, and at that time (more than 60 years ago) little was known about the complexation of aluminum ions studied in detail in later works [12].

Consequently, we come to the conclusion that the values for pH control and prevention of complexation were more accurate in our computer experiments than from Pourbaix's modeling work based on earlier experimental efforts dating back to the 1930s.

Table 1. Chemistry limits (normal range and control conditions) for LDW, PCS, secondary coolant system (SCS), and inside the canal. All data are given in ppm [30].

Normal Range

Water Type	pH	Conductivity	Filterable Solids	Cl-	Activity	Hardness	Trasar	Ortho Phos.	Molybdate
Raw:	~8	~400							
LDW:	5.2-5.8	≤3.0		<0.05	$<1.0\times10^{-3}$				
PCS:	5.1-5.3	2-5	≤0.05	<0.05	<0.16				
SCS:	6.9-7.2	≤2200			$<1.0\times10^{-3}$	≤1200	90-110	7-12	
Anion:	5.2-9.1	≤3.5	<0.08						
Cation:	4.2-5.5	2.5-8.0	<0.08						
Canal	5.2-6.0	≤4.0		<0.05	5.0×10^{-4}				
UCW	6.8-7.8								
HDW:	8.0-10.1				$<2.0\times10^{-4}$				200-300
Demin Water	4.8-6.0								

Control Limits

Water Type	pH	Conductivity	Filterable Solids	Cl-	Activity	Hardness	Trasar	Ortho Phos.	Molybdate
LDW:	5.0-6.0	≤5.0		<0.1	$<1.0\times10^{-3}$				
PCS:	5.0-5.9	<5.0	≤0.1	<0.1	<1.0				
SCS:	6.8-7.3	≤2200			$<1.0\times10^{-2}$	≤1200	85-115		
Anion:	>5.2	<4.0	<0.1						
Cation:	≤5.5	≤10.0	<0.1						
Canal	5.0-6.2	≤5.0		≤2.5	1.6×10^{-3}				
HDW:	7.5-10.5				$<1.0\times10^{-2}$				200-300

Outage Normal range

Water Type	pH	Conductivity
PCS:	5.0-5.8	<8.0

Outage Control limits

pH	Conductivity
4.9-5.9	≤10

Solubility diagrams for boehmite and gibbsite are shown in Figure 8. Note that the minimums for the solubility of boehmite and gibbsite are at slightly different values of pH, and there is an expressed dependence of the results for both substances on temperature – the minimal solubility (inverted peak) moves toward lower values of pH as the temperature increases from 30°C to 50°C. Therefore, when selecting optimized coolant pH value for ATR and other similar research reactors with Al-clad fuel, this fact needs to be borne in mind.

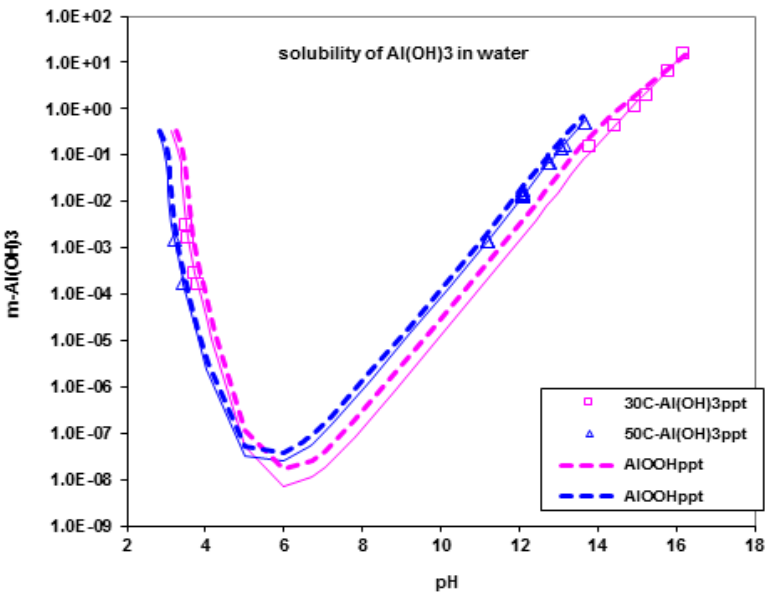

Figure 8. The solubility diagrams for boehmite and gibbsite at 30°C and 50°C. Experimental results [21-22] –squares (experimental) and solid magenta line (modeling) for gibbsite; triangles (experimental) and solid blue line for boehmite.

Our next step was to explore computationally the temperature dependence of the gibbsite solubility on a more systematic basis, Figure 9. The solubility minimum for gibbsite shifts toward more acidic values of pH (from pH~6 at 25°C to pH~5 at 90°C).

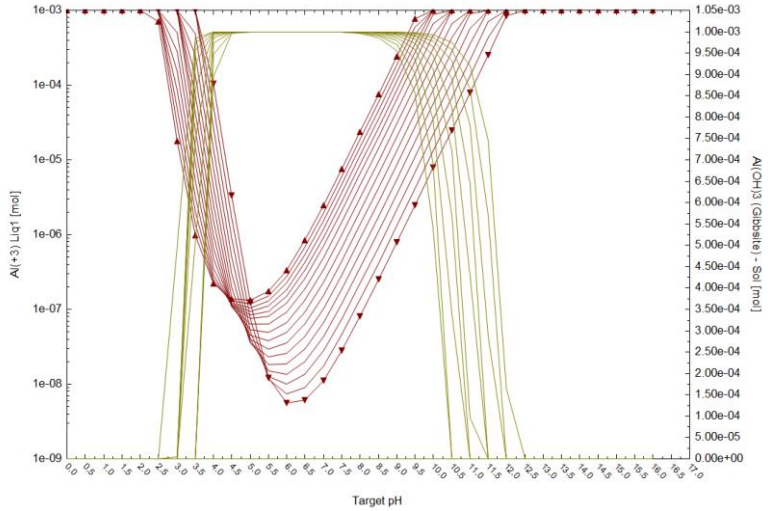

Figure 9. The solubility of gibbsite as a function of pH and temperature (in the 25°C – 90°C range). At the same time, the gibbsite solubility increases with temperature by more than one order of magnitude. These results are in qualitative and quantuitative agreement with those presented in Figure 8.

After all this preparatory work was completed, it was decided to conduct the gibbsite and boehmite solubility studies with higher resolution with respect to pH. The results of these more detailed assessments have yielded the following results, see Figures 10 and 11 for gibbsite and boehmite, respectively. Unfortunately, there is no direct method to simultaneously plot the solubility of gibbsite and

boehmite on the same plot within OLI Studio. As a result, we had to simulate the low pH and high pH regions separately. Then, the results were transferred to Excel for further refinement. These results are presented in Figures 10-11.

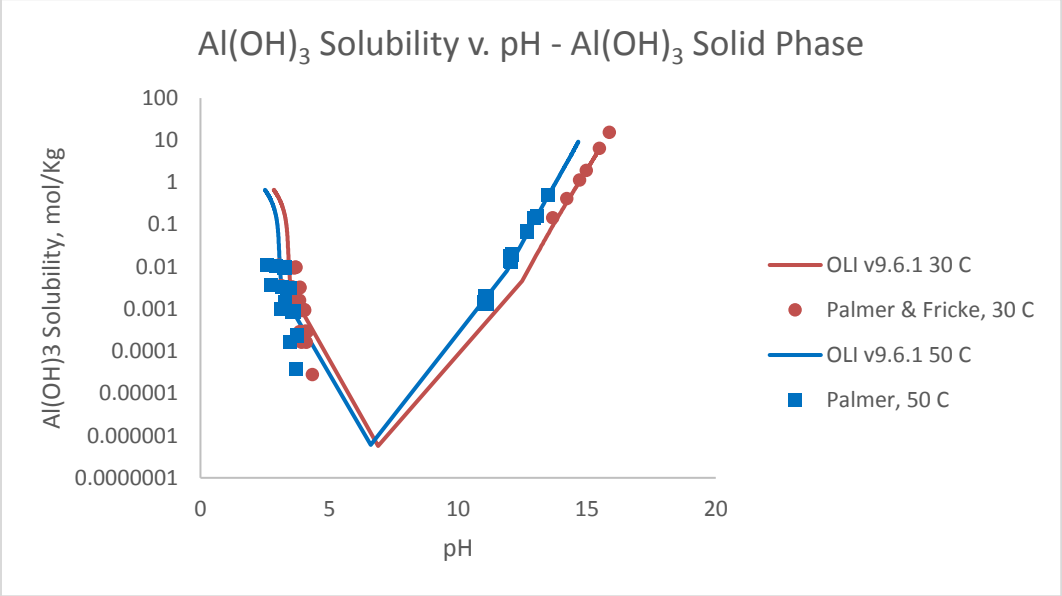

Figure 10. The gibbsite solubility in aqueous solution as a function of pH. Solid lines (brown and blue) illustrate the results of OLI modeling at 30°C and 50°C, respectively. Solid brown circles – experimental results of Palmer and Wesolovski at 30°C [22], solid blue squares – experimental results by Fricke and Jukaitis [27].

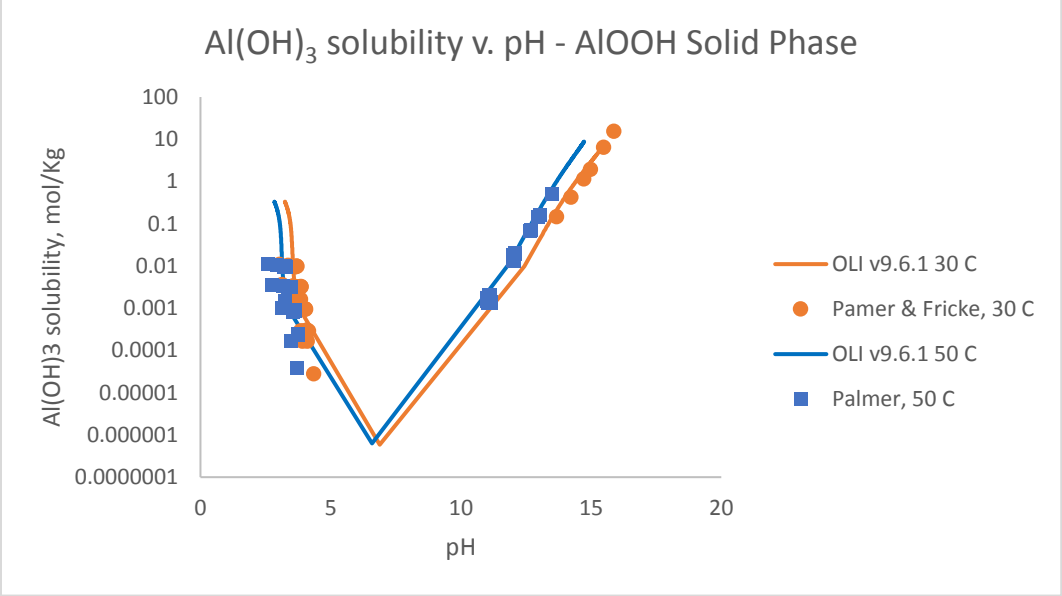

Figure 11. The solubility of boehmite as a function of pH at two temperatures: 30°C and 50°C. Yellow and blue lines – the results of modeling at 30°C and 50°C; yellow circle – experimental data by Palmer and Wesolovski [22] at 30°; blue squares – experimental data by Fricke and Jukaitis at 50°C [27].

Based upon the results presented in Figures 10 and 11, the solubility of $Al(OH)_3$ when the solid phase is either gibbsite or boehmite is similar. As expected, there is more scatter at low pH values than at high pH values. It was also established that some data are available in the mid-pH ranges, but that data was not used in the regressions because of the high degree of scatter and uncertainty. A very similar result was obtained in [31]. That doctoral work was completely devoted to metal hydroxide solubility in aqueous environments, and it was established that virtually all metal hydroxides yield a large amount of scatter in the data near the bottom of these curves [31].

2. THERMAL DEHYDRATION OF SPENT NUCLEAR FUEL: ISSUES RELATED TO ALUMINUM ALLOYS' MICROSTRUCTURE EVOLUTION

2.1 Introduction

At the present time, the only practical way of achieving complete elimination of H_2O (in different forms) is cleaning with subsequent forced thermal dehydration. It is desirable to avoid the purely chemical reaction in dry storage and reduce the potential for different types of corrosion during long term dry storage [32-35]. For example, one such undesirable chemical reaction is the formation of hydrogen:

$6AlO(OH) + 2Al \Rightarrow 4Al_2O_3 + 3 H_2$

Practically no rigorous thermodynamic calculations were reported in the literature pertaining to the possible chemical reactions and/or phase transformations in the SNF. In particular, the temperatures of phase transformations among aluminum oxides, oxy-hydroxides, and hydroxides were reported only as approximate. Consequently, the scientific basis behind the temperatures for the fuel dehydration needs to be established on a quantitative basis. The situation is exacerbated by the need to keep the drying temperature sufficiently low so as to avoid aluminum alloy melting, recrystallization, or changes in its phase composition (see below). For pure aluminum, the melting point is $T_m = 660.3°C$, but in the alloyed state for the AA6061 melting will take place in a temperature range at $T < 580°C$ [36-37]. However, conducting a high-temperature drying would in itself represent a problem for AA6061 because some undesirable microstructure changes could occur.

Depending upon the temperatures of dehydration for different aluminum hydroxides and oxy-hydroxides, **it may not be sufficient** to remove all moisture out of the SNFs prepared for dry storage. Data found in the literature indicate that thermal dehydration of the corrosion products found on the surface of aluminum corroded in water will not produce anhydrous alumina in practical fuel treatment times unless heated to temperatures in excess of about 750 K (477°C) [38-41]. This is in complete agreement with our conclusions made in Part 1 of this report.

2.2 Transition to Dry Storage

At the present time, references were not found regarding the behavior of spent ATR or similar fuel elements in dry storage, but some estimates of the long-term corrosion behavior of aluminum can be derived by inference from other studies. For example, corrosion of pure aluminum was studied for as long as 30 years in atmospheric conditions. It was established that the initial corrosion rate was ~100μm/yr. This corrosion rate decreased to ~3 μm/yr for marine environments. It was established to be even lower (~ 0.8 μm/yr) in a dry and hot climate. These slower, long-term corrosion rates have been observed for periods up to 30 years [37, 42-44].

For alloys of the Al-Mg-Si type, corrosion proceeds in a more complex way because of the formation of the second phase particles (SPPs) in the alloy matrix during heat treatment.

The corrosion of ATR spent nuclear fuel elements in dry storage conditions will depend on a number of the key parameters:

- Integrity of the cladding
- Surface temperature
- Cover gas composition
- Availability of oxygen to the surface
- Adsorbed water on surface
- Humidity conditions
- Corrosion product composition
- Storage container materials.

However, even if the spent fuel is to be stored in a tightly sealed container under an inert gas, it is highly unlikely that the atmosphere over the stored fuel element will be completely dry even after the fuel has gone through a thermal drying process. Consequently, a potential corrosion mechanism will be closer to that found in humid environments at least until all available water is consumed.

2.3 Aluminum Alloy Microstructure Evolution

Below, we consider how microstructure evolves with temperature for the three aluminum alloys used in fuel cladding: the AA5052-H32 (non-heat-treatable Al-Mg alloy); AA1100 (aluminum with minor amounts of Fe and Si); and AA6061 (Al-Mg-Si alloy).

2.3.1 Alloy AA5052-H32

This alloy's chemical composition is given follows: Mg- 2.2 to 2.8 wt.%; Cr -0.15 to 0.35 wt.%; Cu – 0.1 wt.%; Iron – 0.4 wt.% maximum; Mn -0.1 wt.% maximum; Si -0.25 wt.% maximum; Zn – 0.2 wt.% maximum. This alloy's composition, as we as those of the other two alloys considered here, were taken from the Teal Sheets published by the American Aluminum Association [45].

The recently re-assessed Al-Mg and Al-Cu phase diagrams are presented in Figures 12 and 13, [36].

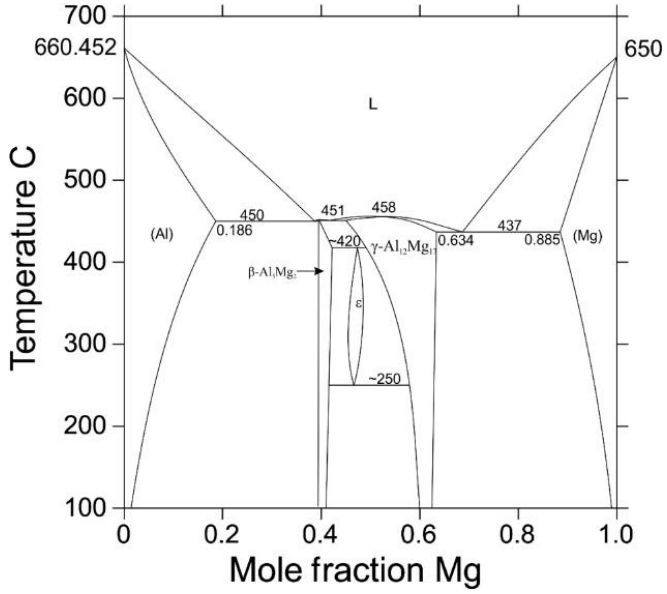

Figure 12. The Al-Mg phase diagram [36] that gives the stoichiometry of the β-phase as Al_5Mg_2.

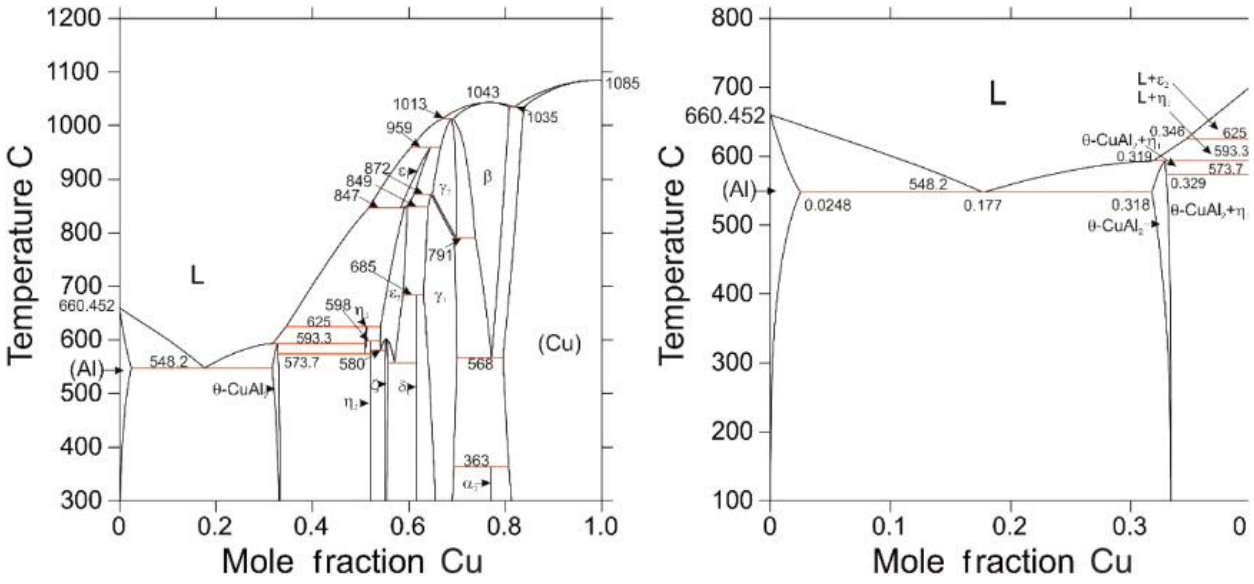

Figure 13. The Al-Cu phase diagrams, where the right diagram shows the relevant low Cu region of the diagram [35].

Using the COST507 thermodynamic database for light alloys [46] and the Thermo-Calc v.2018a software engine [47] we constructed the temperature dependence of alloy's composition, Figure 14. The temperature range is from 100°C to 300°C. From Figure 14 it can be seen that the following phases are present: the FCC Al-matrix (saturated solid solution), Mg_2Si, and intermetallic phases $Al_{13}Cr_2$ and $Al_{13}Fe_4$. Also, there is AlMg_BETA (i.e., Al_8Mg_5), and the TAU phase $Al_{20}Cu_2Mn_3$. The amount of the (Al) solid solution gradually increases in the range from ~100°C to ~180°C, and then remains constant.

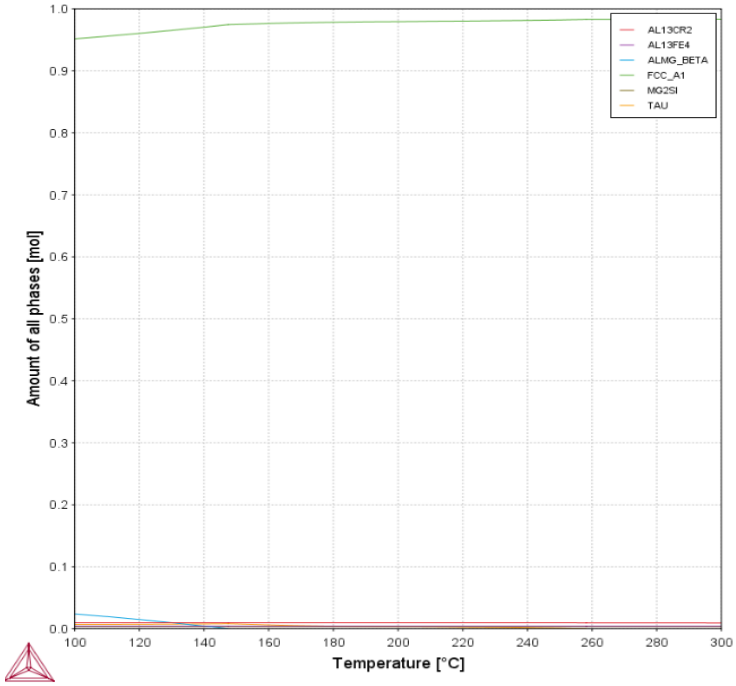

Figure 14. Temperature dependence of the phase composition of the aluminum alloy AA5052.

In Figure 15, the primary (Al) phase is ignored to shows details of the secondary phases.

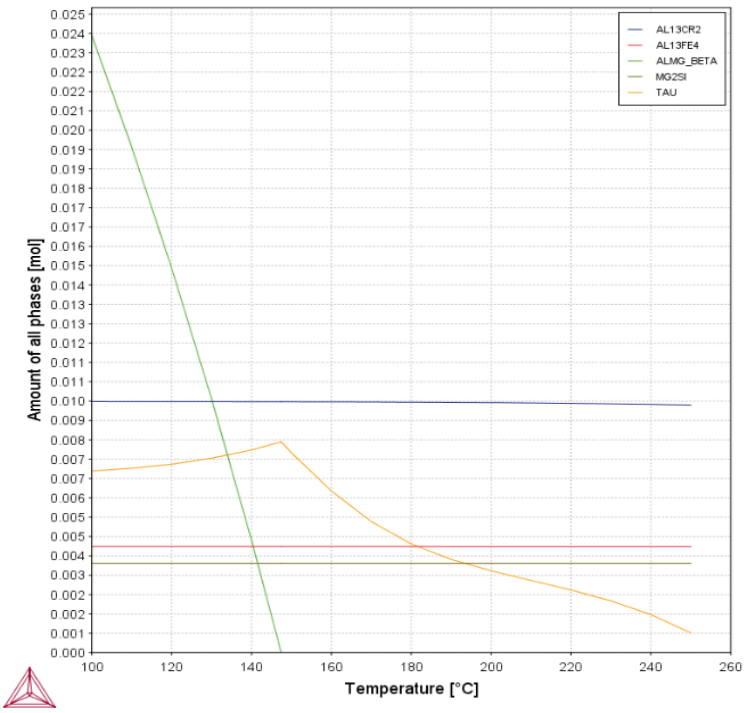

Figure 15. Same as Figure 14, with the concentration range from 0 to 0.025 mol.

Based upon the inspection of Figures 14-15, we can make the following conclusions.

1. The overall amounts of Al_8Mg_5, $Al_{13}Cr_2$, and $Al_{13}Fe_4$ remain practically the same in the temperature range from 100°C to 250°C and higher.
2. The most important phase transformation (from the point of view of the alloy's structural integrity) is the complete disappearance of the Mg_2Si phase and also the gradual variation of the amount of TAU phase taking place in the rage from 100°C to 250°C. At 250°C, the TAU phase disappears completely.
3. However, the actual picture could only be understood if we construct the TTT ("Time-Temperature-Transformation") and CCT ("Continuous Cooling Transformation") diagrams for this system. In other words, the extent to which these phase transformations impact the alloy's structural integrity will be defined by the kinetics of the microstructure evolution processes.
4. This data suggests that the drying temperature for this alloy should not be allowed to exceed 250°C.

2.3.2 Alloy AA6061

Alloy AA6061 belongs to the class of the Al-Mg-Si alloys, with other alloying elements. Since this is the alloy of choice for the nuclear fuel cladding at ATR, we conducted a more detailed study of its microstructure evolution. Both thermodynamic (stable and metastable) and kinetic aspects of microstructural changes as a function of temperature were explored. For that purpose, Thermo-Calc (equilibrium thermodynamics and phase diagrams) [47] and PRISMA software (precipitation calculations - kinetics) [48] were utilized to understand how this alloy's phase composition changes with temperature. Its chemical composition is given below, in weight %: Cr -0.2%; Cu – 0.29%; Fe -0.48%; Mg -1.03%; Mn – 0.04% Si – 0.69%; Ti- 0.02%; Zn – 0.03%; and B – 0.0001% [45].

The results, both for stable phases and metastable phases (primary phase not shown), are given in Figures 16-17.

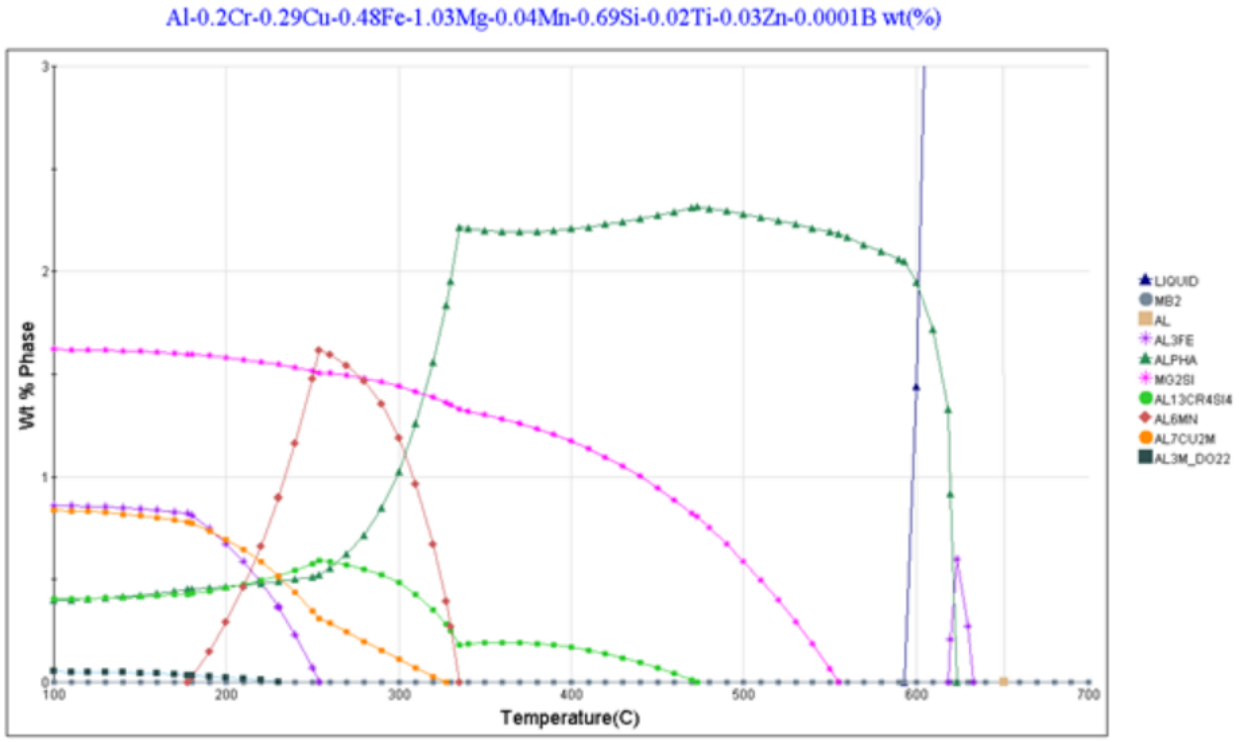

Figure 16. Phase composition of Alloy AA6061 as a function of temperature - equilibrium phases.

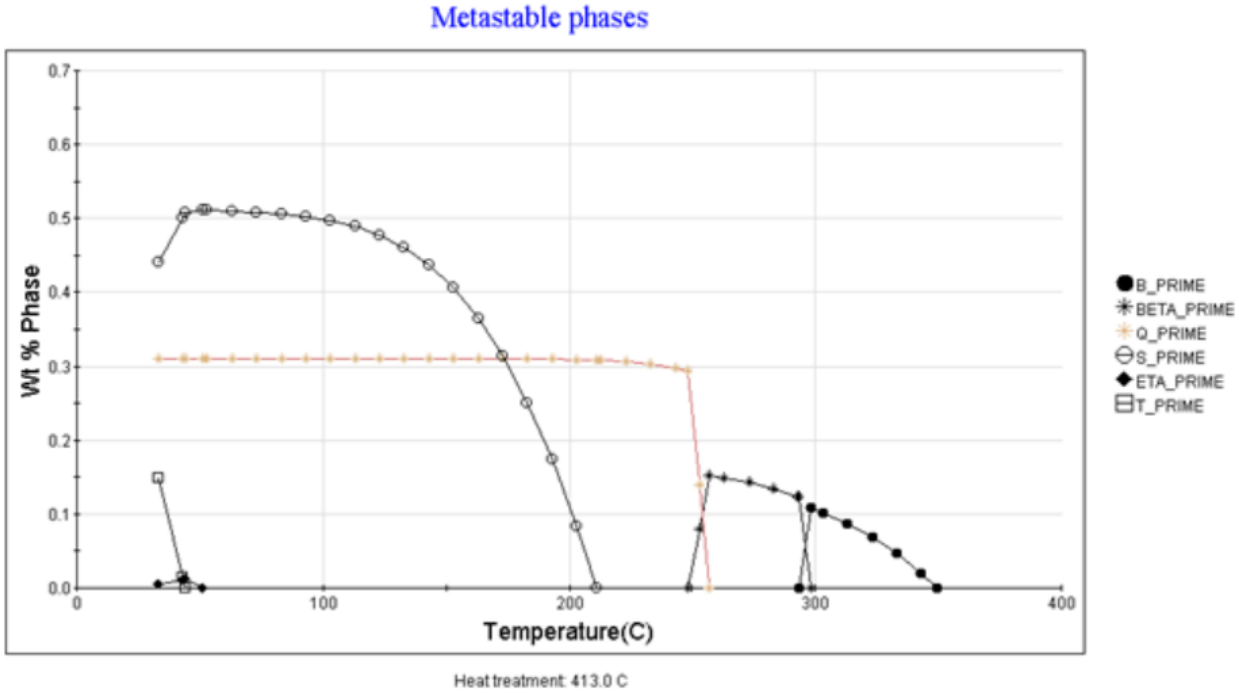

Figure 17. Metastable phases in AA6061 and their evolution with temperature.

Analyzing both diagrams, one can see that quite significant phase transformations start at around 200°C, while at 250°C phase composition changes substantially given enough time for these transformations to occur.

Therefore, at 200°C several phase transformations are to occur potentially (if kinetically allowable):

1. Nucleation and growth of the Al_6Mn phase
2. Decreasing amount of the Al_7Cu_2 phase
3. The onset of changes in the amount of the ALPHA phase (Al_5FeSi)
4. Almost complete disappearance of the metastable S_PRIME phase

At 250°C, there are more phase transformations that may take place. To understand how much time it would take to initiate all these transformations, we have constructed the CCT (Continuous Cooling Diagram) for the AA6061 in Figure 18.

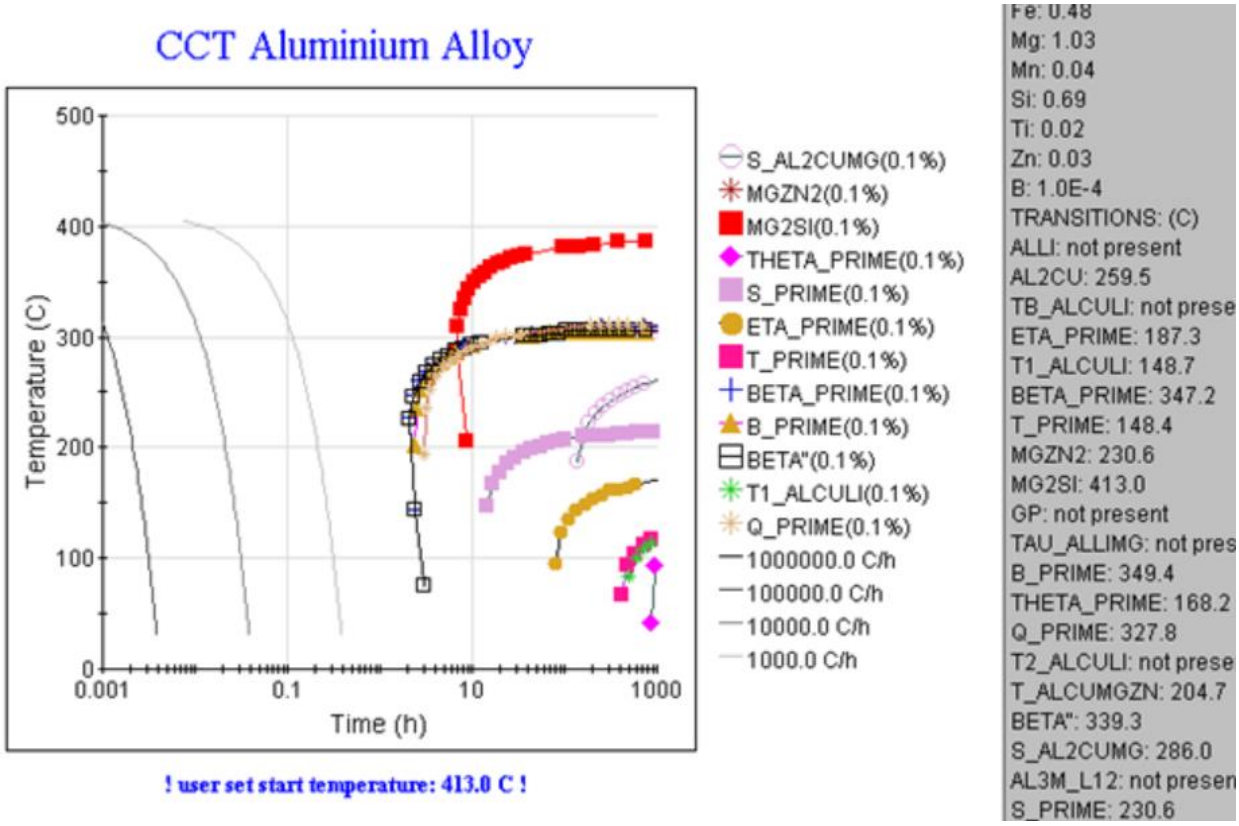

Figure 18. Continuous Cooling Transformation (CCT) diagram for alloy AA6061.

Form this diagram one can see that the "nose" of the diagram is almost at ~220°C. It corresponds to the onset of precipitation of the β"-phase (one of metastable forms of Mg_2Si). Therefore, for the lowest cooling rate (less than 0.3°C per minute) modeled on this diagram, the cooling curve is getting very close to the nose of the CCT diagram. Potential phase transformations that may proceed are given below:

1. Precipitation of β"- a metastable Mg_2Si phase
2. Precipitation of β'- another metastable form of Mg_2Si
3. Precipitation of the Q' –phase

Additionally, it is very important that the diagram in Figure 18 does not account for the irradiation of fuel and the potential appearance of different products of transmutation reactions, up to and including the formation of new phases. In the least, neutron irradiation creates cascades of defects and atomic displacements, which facilitate heterogeneous precipitation of any given phase.

In order to provide a more concise quantitative answer to the extremely important question of potential phase transformations in AA6061, one needs to complete this study and construct the time-temperature transformation (TTT) diagram that will allow assessment of how much time it would take for a particular phase to nucleate and grow at a constant temperature. After that, a correction coefficient based, e.g., on the number of displacements per atom in the fuel and clad will need to be introduced. This is very important because of the dramatic acceleration of all phase transformations under neutron irradiation. For this alloy, the maximal recommended drying temperature should not exceed 220°C.

2.3.3 Alloy AA1100

- Alloy AA1100 has the following composition ranges: Cu – 0.05 −0.20%; Fe −0.95% max; Mn −0.05% max; Si −0.95% max; Zn −0.1% max; Residuals −0.15% max [45]. Therefore, the AA1100 can represent an almost pure aluminum or contain relatively small amounts of other elements. So the following two cases were considered:

  Case 1. Al-99.5%; Fe – 0.5% (lower alloy)

  Case 2. Al - 99.0 %; Fe - 0.4%; Si - 0.4%; Cu - 0.20% (higher alloy)

Case 1. As it follows from Figure 19, the only intermetallic phase is $Al_{13}Fe_4$ and the concentration does not change until approaching the melting point (650°C). Thus it can be safely thermally treated at T = 260°C -280°C, thereby practically ensuring the complete dehydration of both bayerite α-$Al(OH)_3$ and gibbsite (γ-$Al(OH)_3$. We need to worry only about possible recrystallization of this material (change in average grain size), but it will depend upon the reduction ratio when rolling the material down to gage and even with highest reduction does not start developing until 300 - 320°C.

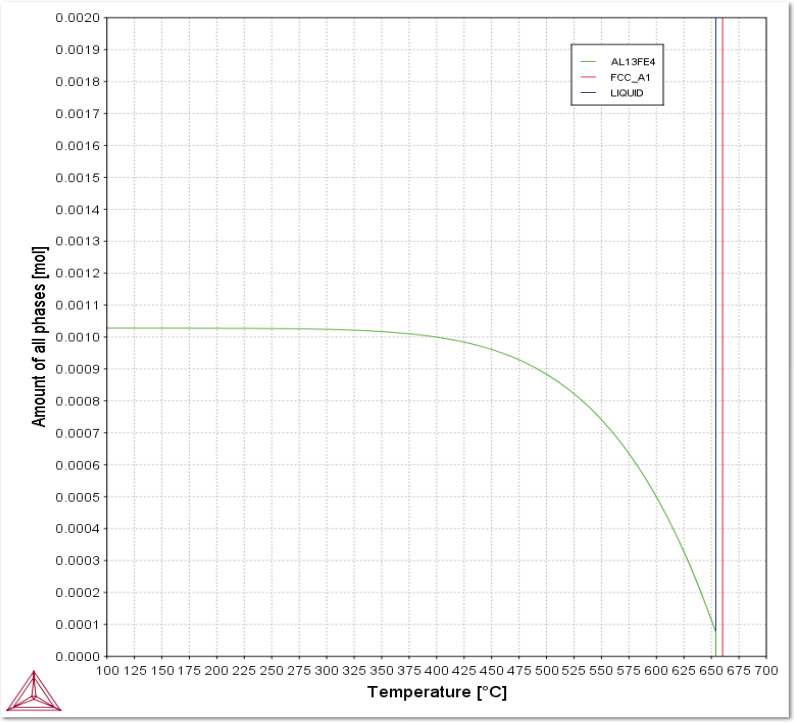

Figure 19. Temperature dependence of the phase composition for alloy AA1100 (Case 1).

The Al-Fe binary phase diagram, recently reassessed [48], is given in Figure 20.

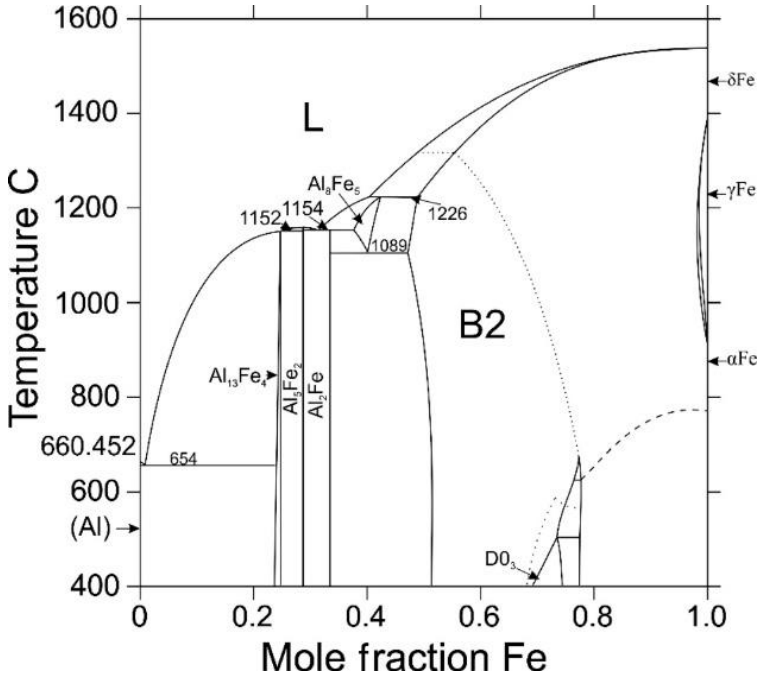

Figure 20. Al-Fe phase diagram illustrating the formation of the $Al_{13}Fe_4$ intermetallic compound [36].

Case 2. The temperature dependence of the phase composition for this case is given in Figures 21-22.

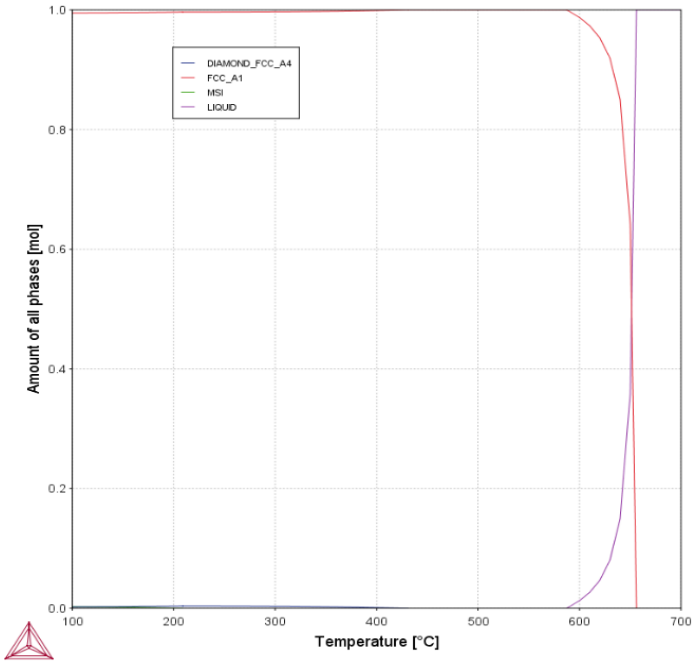

Figure 21. Temperature dependence of the phase composition for alloy AA1100, Case 2.

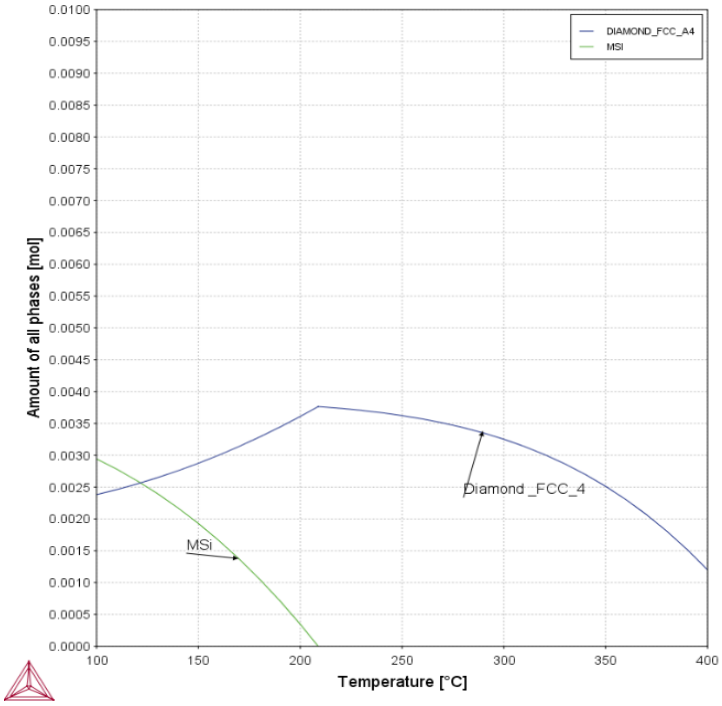

Figure 22. Same Figure 21, for the concentration range from 0 to 0.01 mol.

In this case, the formation of a metal silicide MSi (M=Al, Fe) takes place. Therefore, the amount of the silicide phase is so small that thermal treatment could probably be conducted at temperatures up to 300°C.

To understand this case better, we provide below the Al-Fe-Si-Cu phase diagram, Figure 23 [48].

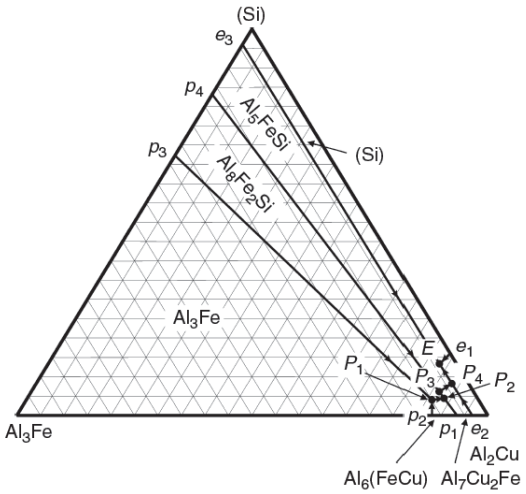

Figure 23. Isothermal section of the AL-Cu-Fe-Si phase diagram in the (Al) corner [48].

Therefore, the "DIAMOND" phase in Figure 22 is pure Si.

Summing up, one can conclude that the AA1100 alloy (in both cases analyzed) is probably the safest in terms of drying SNF at elevated temperatures. Again, one needs to think about recrystallization and not to exceeding ~300°C to avoid grain size changes for the whole crystallographic structure.

3. CONCLUSIONS

In this report, several key scientific issues were identified pertaining to the problem of aluminum spent nuclear fuel (ASNF) and its safe removal from wet storage with subsequent drying and transfer to dry storage at the Department of Energy (DOE) Idaho National Laboratory (INL). It outlines two modeling analyses performed for aluminum and aluminum oxides.

The first analysis examined the solubility of aluminum oxides as a function of temperature and pH. This report presents existing literature produced as far back as the 1950's and including significant analysis and reporting performed at Alcoa in the 1980's. The primary technical gap was the lack of solubility data beyond that reported at standard temperature (25°C). The analysis examined these solubility curves as a function of temperature as well as phase type. The pH value of minimum solubility shifted with temperature but was insensitive to the oxide phase type. The solubility increases with temperature as would be expected, where an order of magnitude increase was observed from 25°C and 90°C. This data provides greater information to understand the various conditions experiences by ASNF including in dry storage in cases where water filming may occur.

A second thermodynamic analysis was performed to examine the aluminum alloy microstructure evolution as a function of temperature. This was performed to understand limitations and possible problems with fuel drying at elevated temperatures. Based on what has been established in previous reports, water remains chemically entrained within boehmite until temperatures exceeding 400°C. Analysis showed that significant phase changes occurred with highly alloyed AA6061 and AA5052 while the more pure aluminum (AA1100) showed nearly inert behavior (i.e. limited phase changes). In the case of the more heavily alloyed AA5052 and AA6061, the phase changes could take place at relatively low temperatures (100°C to 250°C), and thus may have already experienced some of these phase changes in service. As results are thermodynamic in nature, assessment of kinetics will be examined to determine if the phase changes are a concern for the relatively short fuel drying step. This will represent the topic of our future work in this direction.

4. REFERENCES

1. M.J. Connolly, ATR Spent Fuel Management Options Study, INL/EXT-16-40471, (November 2016).
2. L. Lacroix, G. Maxcine Maxted, W. M. Hartman, H.R. Fair, R. Sindelar, W.H. Bates, M.D. Dunsmuir, E.N. Moore, M.C. Chandler, D.B. Rose, M. Connolly, S. Birk, K. Smith, and D. Luke, Aluminum-Clad Spent Nuclear Fuel: Technical Considerations and Challenges for Extended (>50 Years) Dry Storage, Spent Nuclear Fuel Working Group, DOE (2017).
3. R.L. Dillon, Dissolution of Aluminum Oxide as a Regulating Factor in Aqueous Aluminum Corrosion, AEC Research and Development Report, August 31, 1959.
4. D.R. Dickinson and R.J. Lonsibger, Effect of Oxide Dissolution and Heat Transfer on the Corrosion of Aluminum Fuel Cladding, AEC Research and Development Report, December 1963.
5. E. Deltombe and M. Pourbaix, Comportement Elecrochimique de l'Aluminium. Diagrammes d'Equilibres "Tension –pH" du Systeme Al-H_2O a 25°C (Rapport Technique RT.42 of CEBELCOR, December 1955).
6. J.O. Brower, M.V. Glazoff, T.J. Eiden, and A.V. Rezvoi, Evaluation of Corrosion in YA-Type ATR Fuel Element during Reactor PALM Cycle 153B, *Nuclear Technology*, vol. 201, #3, pp.267-286 (March 2018).
7. R. Lowson, Aluminum corrosion studies. I. Potential-pH-temperature diagrams for aluminum. Aust. J. Chem., 27. 10.1071/CH9740105 (1974).
8. C. Misra and K. Wefers, Oxides and Hydroxides of Aluminum, Alcoa Technical Paper #19 (1987).

9. M. Digne, P. Sautet, P. Taybaud, and E. Artacho, Structure and Stability of Aluminum Hydroxides: a Theoretical Study, J. Phys. Chem., v.106, p.5155-5162 (2002).

10. G.V. Franks, Y. Gan, Charging Behavior at the Alumina-Water Interface and Implications f, or Creaming Processing, J. Am. Ceram. Society, v.90 (11), pp.3373-3388 (2007).

11. I. Levin, D. Brandon, Metastable Alumina Polymorphs: Crystal Structures and Transition Sequences, *J. Amer. Ceram. Society*, v.81 (8), pp.1995-2012 (1998).

12. A.K. Karamalidis and D.A. Dzombak, Surface Complexation Modeling: Gibbsite. Wiley, New York (2010).

13. V.S. Zolotorevsky, N.A. Belov, and M.V. Glazoff, Casting Aluminum Alloys, Elsevier, Rotterdam (2007).

14. M.V. Glazoff, A.V. Khvan, V.S. Zolotorevsky, N.A. Belov, and A.Dinsdale, Casting Aluminum Alloys: Their Physical and Mechanical Metallurgy, 2nd edition, Butterworth and Hahnemann, New York (2018).

15. L. Lundberg, Corrosion of Spent ATR Fuel Elements Relative to Their Dry Storage, EG&G ERA-NRE-94-096 (1994).

16. L. Lundberg and M.L. Groson, Corrosion of Spent Advanced Test Reactor Fuel, EGG-M-94222 (1997).

17. R. S. Alwitt, The Aluminum-Water System," Chapter 3 in *Oxides and Oxide Films*, Vol. 4, J. W. Diggle and A.K. Vijh (Eds.), Marcel Dekker, Inc., New York (1976).

18. "Stream Analyzer" software by OLI, LLC (New Jersey) 2018.

19. H.C. Helgeson, D.H. Kirkham, and G.C. Flowers, Theoretical prediction of the thermodynamic behavior of aqueous electrolytes at high pressures and temperatures, IV. Calculation of activity coefficients, osmotic coefficients, and apparent molal and standard and relative partial molal properties to 600°C and 5 kb, *Am. J. Sci.*, v.**281**, p.1249 (1981).

20. J. C. Tanger and H. C. Helgeson, "Calculation of the thermodynamic and transport properties of aqueous species at high pressures and temperatures", *Am. J. Sci.*, v.**288**, p.19 (1988).

21. D.J. Wesolowski, "Aluminum Speciation and Equilibria in Aqueous Solution: I. "The Solubility of Gibbsite in the System Na - K - Cl - OH - $Al(OH)_4$ from 0 to 100°C", Geochimica et Cosmochimica Acta 1992, 56 (3), 1065-1091.

22. D.A. Palmer and D.J. Wesolowski, "Aluminum Speciation and Equilibria in Aqueous Solution: II. The Solubility of Gibbsite in Acidic Sodium Chloride Solutions from 30 to 70°C", *Geochimica et Cosmochimica Acta*, 56 (3) 1093-1111, 1992.

23. M.H. Jung, "Solubility Studies on the $NaAlO_2$-$NaNO_3$-H_2O System", Ms. Thesis, Mississippi State University, December 2005.

24. J.W. Sprauer and D.W. Pearce, "Equilibria in the Systems Na_2O - SiO_2 - H_2O and Na_2O - Al_2O_3 - H_2O at 25°C", Journal of Physical Chemistry 1940, 44 (7), 909-916.

25. A.S. Russell, J.D. Edwards, and C.S. Taylor, "Solubility and Density of Hydrated Aluminas in NaOH Solutions," Journal of Metals 1955, 7, 1123-1128.

26. N.M. Chaplygina, L.S. Itkina, and E.V. Petrova, "Solubility and Solid Phases of the $Al(OH)_3$ - NaOH - H_2O and $Al(OH)_3$ - KOH - H_2O Systems at 50°C", Russian Journal of Inorganic Chemistry 1974, 19(5), 762-766.

27. R. Fricke and P. Jucaitis, "Investigations into the Equation of State in the System Al_2O_3, Na_2O, K_2O, H_2O", Zeitschrift fur Anorganische und Allgemeine Chemie, 191 (1), 129-149, (1930).

28. M. Digne, P. Sautet, P. Taybaud and E. Artacho, "Structure and Stability of Aluminum Hydroxides: a Theoretical Study", J. Phys. Chem., 106, p.5155-5162 (2002).

29. G.V. Franks and Y. Gan, "Charging Behavior at the Alumina-Water Interface and Implications for Creaming Processing", J. Am. Ceram. Society, 90 (11), pp.3373-3388 (2007).

30. INL Electronic Document Management System, Document TOC-191 "ATR Complex OMM-5.1 - Plant Water Chemistry Operating and Maintenance Manual", Rev.55 (06/14/2017).

31. J.A. Dyer, "Advanced Approaches for Modeling Trace Metal Sorption in Aqueous Systems", Ph.D. Dissertation, University of Delaware (2003).

32. D.R. Dickinson and R.J. Lonsibger, "Effect of Oxide Dissolution and Heat Transfer on the Corrosion of Aluminum Fuel Cladding", AEC Research and Development Report, December 1963.

33. S.P. Henslee, "ATR Fuel Element Pitting", EG&G PR-T-80-030, April 1980 Also see: K. Vinjamuri, "Post-Irradiation Examination of Advanced Test Reactor Fuel Elements", EG&G-TFBF-5968, September 1982.

34. L. Lundberg, "Corrosion of Spent ATR Fuel Elements Relative to Their Dry Storage", EG&G ERA-NRE-94-096 (1994); also see: L. Lundberg and M.L. Groson, "Corrosion of Spent Advanced Test Reactor Fuel", EGG-M-94222 (1997).

35. D. Illum, "ATR Fuel Summary Report", INEL-96/300, September 1996.

36. M.E. Glicksman, Principles of Solidification: An Introduction to Modern Casting and Crystal Growth Concepts, Springer, Berlin, (2010).

37. E. Shaber, G. Hoffman (ANL), "Corrosion Minimization for Research Reactor Fuel", INL/EXT-05-00256, June 2005.

38. "Corrosion Analysis for non-Dried ATR Aluminum Fuel Plate Fuels Placed in CS Canisters", EDF-7936, Idaho Cleanup Project, May 22, 2007.

39. Y.S. Kim, G.L. Hofman, A.B. Robinson, J.L. Snelgrove, and N. Hanan, "Oxidation of Aluminum Alloy Cladding for Research and Test Reactor Fuel", Journal of Nuclear Materials, 378 (2008) 220-228.

40. J.G. Kaufman, E.L. Rooy, Aluminum Alloy Castings: Properties, Processes, and Applications, ASM International, Metals Park, OH, (2004).

41. "Nuclear Corrosion Science and Engineering", Ed. By Damien Feron, Woodhead Publishing, vol. 22 Philadelphia (2012).

42. D.A. Jones, "Principles and Prevention of Corrosion", Macmillan, New York (1992).

43. "Corrosion of Research Reactor Aluminum Clad Spent Fuel in Water", IAEA Technical Report Series, Report no. 418, Chapter 3; Guidelines for Corrosion Protection of Research Reactor Aluminum Clad Spent Nuclear Fuel in Interim Wet Storage, pg. 56-60, Vienna (2003).

44. D.G. Eskin, Physical Metallurgy of Direct Chill Casting of Aluminum Alloys, CRC Press, Boca Raton, FL, (2008).

45. www.thermocalc.com Thermo-Calc AB, Stockholm, Sweden (2018).

46. Sente Software Inc., Cambridge, UK.